Synthesis and characterization of $BaIn_{0.3-x}Y_xCe_{0.7}O_{3-\delta}$ (x=0, 0.1, 0.2, 0.3) proton conductors

Fei Zhao[1], Qiang Liu[1], Siwei Wang[1], Kyle Brinkman[2], Fanglin Chen[1]*

[1]Department of Mechanical Engineering, University of South Carolina,

Columbia, SC 20208, USA

[2] Materials Science and Technology Directorate, Savannah River National Laboratory

(SRNL) Aiken, SC 29803, USA

[*]Corresponding Author:

Fanglin Chen*

Department of Mechanical Engineering, University of South Carolina, Columbia, SC

20208, USA

(Tel.) 803-777-4185; (fax) 803-777-0106

(E-mail): chenfa@cec.sc.edu

Abstract

The morphological and electrical properties of yttrium (Y) and indium (In) doped barium cerate perovskites of the form $BaIn_{0.3-x}Y_xCe_{0.7}O_{3-\delta}$ (with x=0-0.3) prepared by a modified Pechini method were investigated as potential high temperature proton conductors with improved chemical stability. The sinterability increased with the increase of In-doping, and the perovskite phase was found in the $BaIn_{0.3-x}Y_xCe_{0.7}O_{3-\delta}$ solid solutions over the range $0\leq x\leq0.3$. The conductivities decreased (from x to x, insert quantitative values) while the tolerance to wet CO_2 improved for $BaIn_{0.3-x}Y_xCe_{0.7}O_{3-\delta}$ samples with an increase of In-doping.

1. Introduction

In the past two decades, high temperature proton conductors with the ABO_3 perovskite structure, such as $BaCeO_3$, $BaZrO_3$, $SrCeO_3$ and $SrZrO_3$ have been extensively studied due to the low activation energy and high proton conductivity [2-4]. Among them, doped barium cerates, $BaCe_{1-x}A_xO_{3-\delta}$ (A = Y^{3+}, In^{3+}, rare-earth ions such as Nd^{3+}, Sm^{3+}, Gd^{3+}, Eu^{3+} and Yb^{3+}, $\delta = x/2$) have exhibited particularly high proton conductivity [10-16]. In general, the highest proton conductivity among the barium cerates and zirconates has been observed with Y^{3+} doping, followed by Gd^{3+} and other lanthanides [3, 5, 7]. The increase in proton conductivity with doping is mainly related to the formation of protonic defects in the ABO_3 perovskites due to

dissociative adsorption of water in the presence of oxygen vacancies. In the case of Y-doped BaCeO₃, the creation of oxygen vacancies through the defect reaction can be written in the Kroger–Vink notation as:

$$2Ce_{Ce}^{x} + Y_2O_3 + O_O^{x} \rightarrow 2Y_{Ce}^{'} + V_O^{\bullet\bullet} + 2CeO_2 \quad (1)$$
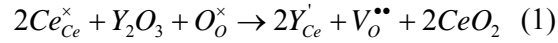
and the formation of hydroxyl ions with oxygen vacancies constituting the site for the incorporation of water through:

$$H_2O(g) + V_O^{\bullet\bullet} + V_O^{x} \rightarrow 2OH_O^{\bullet} \qquad\qquad (2)$$

The mechanism of proton migration by a series of jumps from one position to the next position in perovskite oxides was proposed by Iwahara [7] and further analyzed by Kreuer [5]. Oxygen vacancies are the main defects at high temperatures where water molecule desorption takes place, together with oxygen migration in the bulk while the dissolution of protons is favoured by decreasing temperatures. The proton conduction becomes predominate at intermediate temperatures near 600°C.

High temperature proton conductors have a wide range of applications. Firstly, they can be used as electrolytes for solid oxide fuel cells (SOFCs). SOFC is an energy conversion device that directly produces electricity by electrochemical combination of a fuel and an oxidant with high efficiency and extremely low to zero emissions [1]. They can also be used as membranes for hydrogen separation, enabling the production of high purity hydrogen from coal gasified gas streams. Hydrogen is an attractive fuel for both the electric power and transportation industries due to carbon free combustion products which address rising concerns over the global climate change. In

addition, high temperature proton conductors may play an important role in the next generation nuclear power plant since they can be used to isolate hydrogen contaminants present in the helium gas streams utilized for reactor cooling. In all of the above applications, high proton conductivity and good chemical stability are required to enhance the device performance.

Although Y-doped $BaCeO_3$ possesses the highest proton conductivity among all perovskite-type high temperature proton conducting oxides studied so far, barium cerates can easily decompose into barium carbonate (or barium hydroxide) and cerium oxide at elevated temperatures in CO_2 and or in humid atmospheres. Consequently, recent works have been focused on the development and optimization of the performance of doped cerates in order to enhance their chemical stabilities without remarkably sacrificing their proton conductivities. [5, 17, 18]. Among the different strategies exploited, the most popular approach is to prepare mixed barium cerate/barium zirconate solid solution. Although zirconate-based proton conductors are relatively more stable at elevated temperatures in CO_2 and or in humid atmospheres, they have much lower conductivity. $BaCeO_3$ and $BaZrO_3$ can easily form a solid solution across the entire composition range. Consequently, it might be possible to replace a fraction of Ce in $BaCeO_3$ with Zr, thereby achieving a solid solution of cerate and zirconate with both good protonic conductivity and chemical stability. Further it has been recently reported that a Zr-free barium cerate (i.e. In-doped $BaCeO_3$) possesses good stability at elevated temperatures in CO_2 and

H$_2$O-rich environments [19, 20]. However, the electrical conductivity of In-doped BaCeO$_3$ proton conductors is relatively low [11, 21]. To improve the conductivity of In-doped BaCeO$_3$ proton conductor, yttrium could be used as dopant instead of indium since yttrium doped BaCeO$_3$ has high conductivity among doped BaCeO$_3$. In this work, BaIn$_{0.3-x}$Y$_x$Ce$_{0.7}$O$_{3-\delta}$ (BIYC, x=0, 0.1, 0.2, 0.3) solid solutions prepared by a modified Pechini method have been investigated to find a composition having both high conductivity and good stability.

2. Experimental

2.1 Fabrication of perovskite powders

Powder samples of barium cerate solid solutions having the nominal composition of BaIn$_{0.3-x}$Y$_x$Ce$_{0.7}$O$_{3-\delta}$ (x=0, 0.1, 0.2, 0.3) were synthesized by a sol–gel modified Pechini process to ensure a good homogeneity of the mixed oxides. The starting materials were Ba(NO$_3$)$_2$ (Alfa Aesar, 99.95%), Ce(NO$_3$)$_3$·6H$_2$O (Alfa Aesar, 99.5%), In(NO$_3$)$_3$·4.7H$_2$O (Alfa Aesar, In 29% min), and Y(NO$_3$)$_3$·6H$_2$O (Alfa Aesar, 99.9%) as metal precursors and EDTA (Ethylenediaminetetraacetic acid, Alfa Aesar, 99%) and citric acid (Alfa Aesar, 99%) as chelating and complexing agents, respectively. The water content of the indium salt was determined by thermogravimetric analysis. Ammonium hydroxide (Sigma-Aldrich, NH$_3$ content 28.0 to 30.0%) was added to promote the dissolution of EDTA in deionized water. An appropriate amount of barium nitrate was first dissolved in deionized water. Following that, an aqueous solution of EDTA and ammonia (pH~9) was added drop wise to the barium solution.

The mixture was kept at 50°C with mild continuous stirring until a clear solution was obtained. An aqueous solution containing stoichiometric amounts of cerium, indium and yttrium salts was subsequently slowly added to the barium nitrate solution. Finally, an appropriate amount of citric acid was added (citric acid : metal nitrates : EDTA molar ratios = 1.5 : 1 : 1) and the final solution was stirred at room temperature for 24 h. Water was then slowly evaporated on a hot plate and the resulting brown gel was dried at 300°C. The dried ashes were then treated at 600°C in air for 2 hour (heating rate 3°C min^{-1}) to remove the organic residue. The temperature of the thermal treatment was chosen based upon thermogravimetric analyses performed on the as-prepared precursor with flowing air. Fine $BaIn_{0.3-x}Y_xCe_{0.7}O_{3-\delta}$ powders were obtained by calcination the heat treated powders at 1000°C in air for 6 h (heating rate 3°C min^{-1}).

2.2 Conductivity measurement

The resulting fine powders were uni-axially pressed into pellets at 400 MPa. The pellets were sintered at 1450°C for 5 hours in air and the crystalline structure of the sintered samples was measured using a X-ray powder diffractometer (Mini X-ray diffractometer with graphite-monochromatized Cu Kα radiation (λ=1.5418 Å)), employing a scanning rate of 10 $^{\circ}$/min in the 2θ range of 20 to 80°. Densification studies were performed by direct measurements of sample dimensions and weight and by linear shrinkage after sintering. Morphological investigations on the prepared powder and sintered disks were based on the scanning electron microscopy (SEM)

observations by a FEI Quanta and XL 30 model. For electrochemical measurement, both sides of the disks were polished with 400 grade SiC sandpaper and then cleaned in an ultrasonic cleaner. Platinum paste (Heraeus, component metallization CL11-5349) was painted on both sides of the samples, and then sintered at 1000°C for 1 h to form a porous platinum electrode. Platinum wires were attached to the surface of pellet. Electrical conductivity was measured by A.C. impedance method. A.C. impedance responses were collected with the A.C. amplitude of 10mV in the frequency range between 0.01 Hz and 1 MHz by a electrochemical station (Metek, Versa STAT3-400) in different atmospheres at 500-800°C (50°C per step). From the intercepts of impedance plots with the real axis, the ohmic resistance of the samples can be determined. The total conductivity is obtained using the following equation: $\sigma=L/(RS)$, where σ is the conductivity, L is the sample thickness, R is the ohmic resistance and S is the Pt electrode area.

3. Results and discussion

Fig. 1 shows the XRD data for $BaIn_{0.3-x}Y_xCe_{0.7}O_{3-\delta}$ as a function of the Y content. A single phase perovskite structure was obtained for most of these compositions. For the In-doped materials, $BaIn_{0.3}Ce_{0.7}O_{3-\delta}$ was determined to be an orthorhombic *Pmcn* unit cell even when the In^{+3} content was increased up to 30%, as reported by Giannici [22]. However, for the Y-doped barium cerate, the Y dopant solubility limit is less than 20% of the available Ce sites. Consequently, the Y_2O_3 phase segregated at the grain boundaries in $BaY_{0.3}Ce_{0.7}O_{3-\delta,}$ as can be seen from the XRD pattern in Fig. 1.In

addition, it was observed that Y^{3+} adapts poorly to insertion in the host lattices in cerate due to its very high hardness. On the other hand, In^{3+}, being much softer than Y^{3+} (i.e., more easily polarized), can be more effectively inserted in the host lattices since its low hardness allows for the release of the resulting strain, and consequently stabilizes the structure.

To investigate the sinterability of the In-doped powders, morphologies of the powders and sintered ceramics were analyzed by SEM. As shown in Fig. 2, the SEM image of the $BaIn_{0.3}Ce_{0.7}O_{3-\delta}$ powder calcined at $1000^{o}C$ for 6 h in air reveals a network-like morphology, and plenty of voids are distributed inside a foam-like structure. The morphologies for the other BICY powders with different compositions were similar. Such fluffy powders having very low filled density are particularly suitable for fabricating thin membranes by a dry-pressing method. After sintering the BICY pellets at $1450^{o}C$ for 5h, the size of crystalline grains and the number of closed pores increase with Y doping content as shown from the cross-sectional views of those ceramic disks in Fig. 3. The average grain size is determined using a linear intercept method by counting the adjacent grains in the SEM. The average grain sizes are 5.6, 8.5, 12.7 and 15.2μm for $BaIn_{0.3-x}Y_xCe_{0.7}O_{3-\delta}$ (x=0, 0.1, 0.2, 0.3) samples, respectively. And the packing between $BaIn_{0.3}Ce_{0.7}O_{3-\delta}$ crystallites is more compact than that of $BaY_{0.3}CeO_{3-\delta}$, which is consistent with the shrinkage results of those sintered pellets. After sintering at $1450^{o}C$ for 5h, the linear shrinkages of the disk diameters are 12.3%, 12.0%, 11.5% and 10.3% for $BaIn_{0.3-x}Y_xCe_{0.7}O_{3-\delta}$ (x=0, 0.1, 0.2, 0.3) samples,

respectively. The results of Archimedes's water displacement measurements on the sintered disks showed that all the relative densities were higher than 94% for BIYC sintered samples. Consequently, In-doping results in an improved sinterability of $BaY_{0.3}CeO_{3-\delta}$.

To investigate the chemical stability of the $BaIn_{0.3-x}Y_xCe_{0.7}O_{3-\delta}$ (x=0, 0.1, 0.2, 0.3), the BICY disks were exposed to wet 3vol% CO_2 (air as the balance gas, 3vol% H_2O) with a flow rate of 40 mLmin^{-1} at 700°C for 24 h. The formation of $BaCO_3$ and CeO_2 can be observed in the XRD patterns shown in Fig. 4. The number and intensity of the impurity peaks was observed to decrease with Y doping, suggesting that the tolerance to CO_2 decreased with Y doping for $BaIn_{0.3-x}Y_xCe_{0.7}O_{3-\delta}$ (x=0, 0.1, 0.2, 0.3) ceramics. For example, although the main perovskite structure phase of BICY remains, the reaction between $BaY_{0.3}Ce_{0.7}O_{3-\delta}$ and wet CO_2 is more severe than $BaIn_{0.3}Ce_{0.7}O_{3-\delta}$. This can give rise to a loss of cell performance resulting from the conductive degradation by the appearance of additional phases, indicating that the high doping level of Y decreases the chemical stability of BICY ceramics.

Shown in Fig. 5 are the conductivities of the $BaIn_{0.3-x}Y_xCe_{0.7}O_{3-\delta}$ (x=0, 0.1, 0.2, 0.3) samples in different atmospheres in the temperature range of 550-800°C. Among all the samples examined, $BaY_{0.3}Ce_{0.7}O_{3-\delta}$ shows the highest conductivities: 3.36×10^{-2}, 3.5×10^{-2}, 2.40×10^{-2} and 2.71×10^{-2} Scm^{-1} in dry air, wet air, wet nitrogen and wet hydrogen at 800°C, respectively. At a given operating temperature, the conductivities of BICY samples increased with the amount of Y doping. From the change of slope

coefficient shown in Fig. 5(1) and (3), it indicates that the activation energies for total conductivity of the $BaIn_{0.3-x}Y_xCe_{0.7}O_{3-\delta}$ system in dry air and wet N_2 has a slight tendency to decrease with the increase of the Y content. The conductivities of all samples in wet hydrogen (Fig. 5(4)) are found to be lower than those in dry (Fig. 5(1)) and wet (Fig. 5(2)) air, probably due to the presence of ionic and hole conductivity in air since the hole conductivity depends on the oxide ion vacancy concentration introduced through doping with trivalent ions and on oxygen partial pressure [24]. Meanwhile, the turning lines in Fig. 5(2) for the In-doped samples in the temperature regions (650-800 ^{o}C) could be probably due to the change of the conduction mechanism when water vapor and air are present, derived from the change of the effective charge carriers' concentration [25, 26].

4. Conclusions

In summary, $BaIn_{0.3-x}Y_xCe_{0.7}O_{3-\delta}$(x=0, 0.1, 0.2, 0.3) powders have been successfully synthesized by a modified Pechini method. An increase in the yttrium content in $BaIn_{0.3}Ce_{0.7}O_{3-\delta}$ resulted in enhanced conductivity in both dry air and wet hydrogen,the highest conductivity was observed for x=0.3 (x S/cm). The sinterability of $BaIn_{0.3-x}Y_xCe_{0.7}O_{3-\delta}$(x=0, 0.1, 0.2, 0.3) decreased with the increase in Y doping content. However, tolerance to wet CO_2 for $BaIn_{0.3-x}Y_xCe_{0.7}O_{3-\delta}$ samples decreased with the increase of the amount of Y doping.

References

[1] N.Q. Minh, J.Am.Ceram.Soc. 76 (1993) 563-588.

[2] N. Bonanos, B. Ellis, M.N. Mahmood, Solid State Ionics 44 (1991) 305.

[3] A.S. Nowick, Y. Du, Solid State Ionics 77 (1995) 137-146.

[4] N. Bonanos, K.S. Knight, B. Ellis, Solid State Ionics 79 (1995) 161-170.

[5] K.D. Kreuer, Annu. Rev. Mater. Res. 33 (2003) 333-359.

[6] H. Iwahara, T. Esaka, H. Uchida, N. Maeda, Solid State Ionics, 3/4 (1981) 359-363

[7] H. Iwahara, Solid State Ionics 86-88 (1996) 9-15.

[8] K.D. Kreuer, Chem. Mater. 8 (1996) 610-641.

[9] F. Lefebvre-Joud, G. Gauthier, J. Mougin, J. Appl. Electrochem. 39 (2009) 535-543.

[10] A.N. Virkar, H.S. Maiti, J. Power Sources 14 (1985) 295-303.

[11] K. Künstler, H.J. Lang, A. Maiwald, G. Tomandle, Solid State Ionics 107 (1998) 221-229.

[12] F.L. Chen, O. Toft Sørensen, G.Y. Meng, D.K. Peng, Journal of the European Ceramic Society 18 (1998) 1389-1395.

[13] Z.L. Wu, M.L. Liu, J. Electrochem. Soc. 144(6) (1997) 2170-2175.

[14] R.R. Peng, Y. Wu, L.Z. Yang, Z.Q. Mao, Solid State Ionics 177 (2006) 389-393.

[15] S. Yamaguchi, N. Yamada, Solid State Ionics 162-163 (2003) 23-29.

[16] J.X. Wang, L.P. Li, B.J. Campbell, Z. Lv, Y. Ji, Y.F. Xue, W.H. Su, Materials Chemistry and Physics 86 (2004) 150-155.

[17] S.M. Haile, G. Staneff, K.H. Ryu, J. Mater. Sci. 36 (2001) 1149-1160.

[18] E. Fabbri, A. D'Epifanio, E. Di Bartolomeo, S. Licoccia, E. Traversa, Solid State Ionics 179 (2008) 558-564.

[19] N.I. Matskevich, Journal of Thermal Analysis and Calorimetry 90 (2007) 955-958.

[20] L. Bi, S.Q. Zhang, L. Zhang, Z.T. Tao, H.Q. Wang, W. Liu, International Journal of Hydrogen Energy 34 (2009) 2421-2425.

[21] H. Matsumoto, Y. Kawasaki, N. Ito, M. Enoki, T. Ishihara, Electrochem. and Solid-State Lett. 10(4) (2007) B77-B80.

[22] F. Giannici, A. Longo, A. Balerna, K.D. Kreuer, A. Martorana, Chem. Mater. 19 (2007) 5714-5720.

[23] H. Iwahara, Solid State Ionics 52 (1992) 99-104.

[24] T. Shimura, H. Tanaka, H. Matsumoto, T. Yogo, Solid State Ionics 176 (2005) 2945–2950.

[25] E. Gorbova, V. Maragou, D. Medvedev, A. Demin, P. Tsiakaras, Journal of Power Sources 182(2) (2008) 207-213.

[26] J.R. Frade, Solid State Ionics 78 (1995) 87-97.

Figure captions

Fig. 1 XRD patterns of $BaIn_{0.3-x}Y_xCe_{0.7}O_{3-\delta}$ (x=0, 0.1, 0.2, 0.3) powders sintered at 1450^oC for 5h in air. *: Y_2O_3

Fig. 2 SEM photograph of $BaIn_{0.3}Ce_{0.7}O_{3-\delta}$ powder sintered at 1000^oC for 6h in air.

Fig. 3 The cross-sectional views of different pellets after sintering at 1450^oC for 5h in air. (1) $BaIn_{0.3}Ce_{0.7}O_{3-\delta}$ (2) $BaIn_{0.2}Y_{0.1}Ce_{0.7}O_{3-\delta}$ (3) $BaIn_{0.1}Y_{0.2}Ce_{0.7}O_{3-\delta}$ (4) $BaY_{0.3}Ce_{0.7}O_{3-\delta}$.

Fig. 4 XRD patterns of $BaIn_{0.3-x}Y_xCe_{0.7}O_{3-\delta}$ (x=0, 0.1, 0.2, 0.3) disks measured on the surfaces after exposure to wet 3% CO_2 with air as the balance gas at 700^oC for 24h. *: $BaCO_3$, o: CeO_2.

Fig. 5 Effect of temperature on the conductivity of the $BaIn_{0.3-x}Y_xCe_{0.7}O_{3-\delta}$ (x=0, 0.1, 0.2, 0.3) samples in dry air (1), wet air (2), wet nitrogen (3) and wet hydrogen (4).
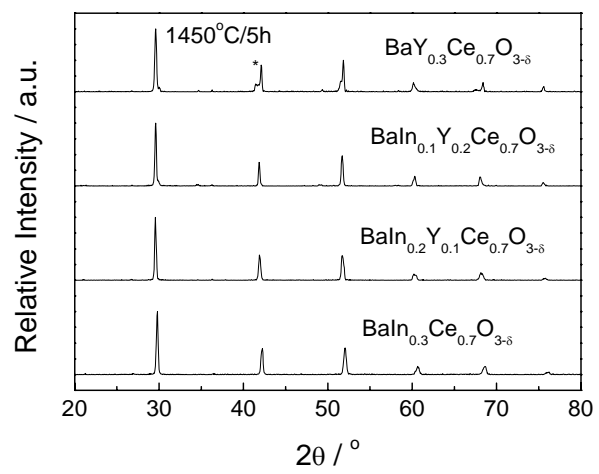
Figures

Fig. 1

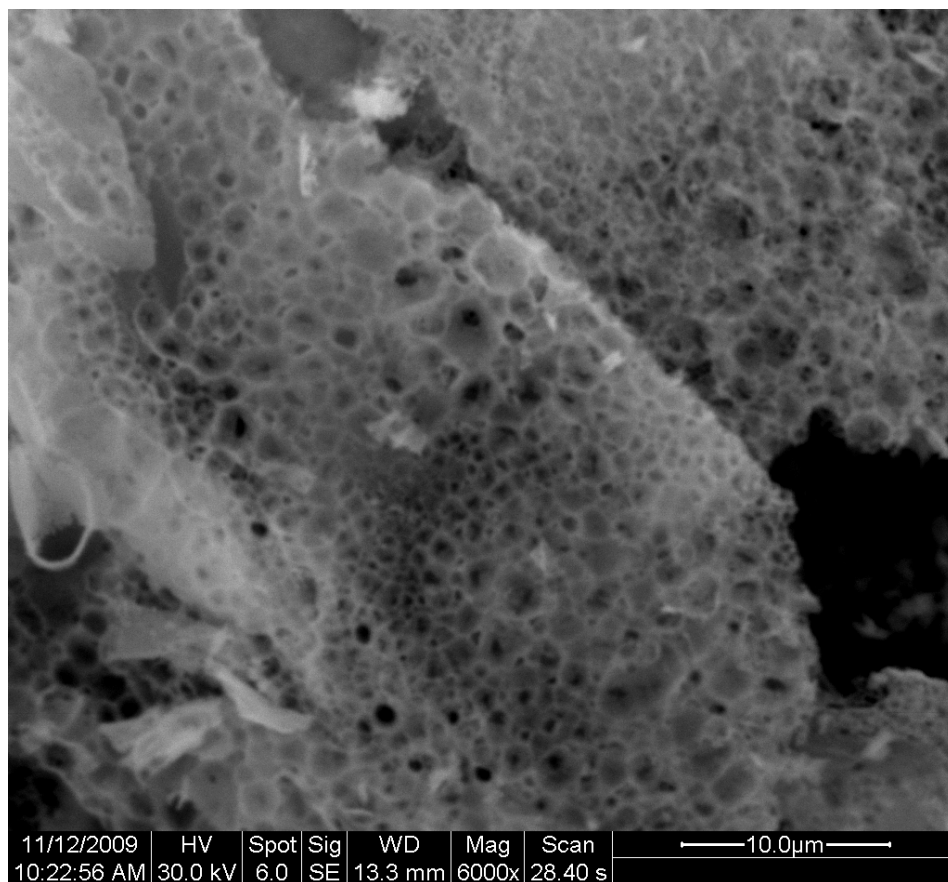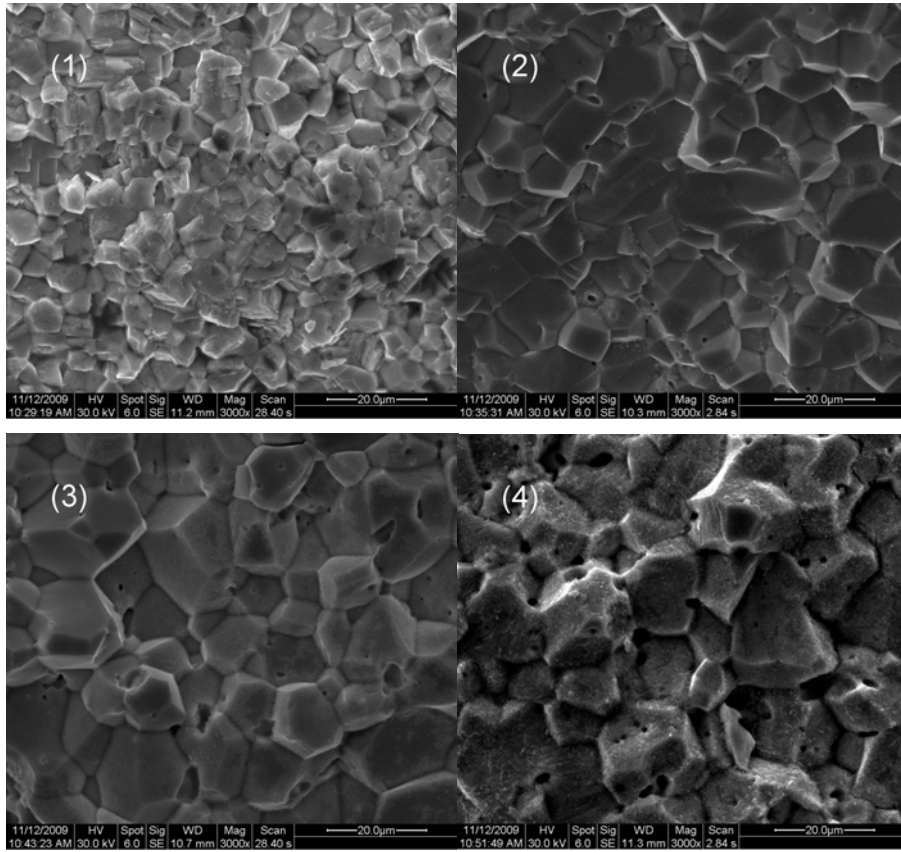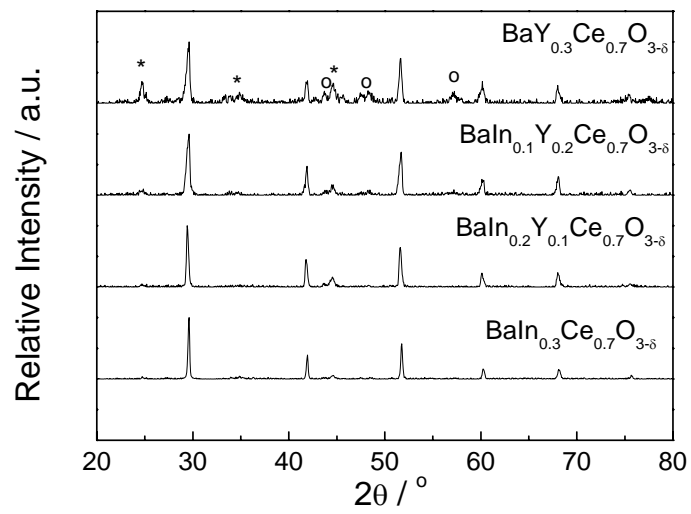| 11/12/2009 | HV | Spot | Sig | WD | Mag | Scan | 10.0μm |
| 10:22:56 AM | 30.0 kV | 6.0 | SE | 13.3 mm | 6000x | 28.40 s | |

Fig. 2

Fig. 3

Fig. 4

Fig. 5